



Experimental and numerical study on the transient behavior of partial oxidation of methane in a catalytic monolith

Renate Schwiedernoch, Steffen Tischer, Chrys Correa, Olaf Deutschmann*

IWR, Heidelberg University, Im Neuenheimer Feld 368, D-69120 Heidelberg, Germany

Abstract

The objective of this investigation is a better understanding of transient processes in catalytic monoliths. As an example, the light-off of the partial oxidation of methane to synthesis gas (H_2 and CO) on a rhodium/alumina catalyst is studied experimentally and numerically.

Methane/oxygen/argon mixtures are fed at room temperature and atmospheric pressure into a honeycomb monolith, which is pre-heated until ignition occurs. The exit gas-phase temperature and species concentrations are monitored by a thermocouple and mass spectroscopy, respectively. In the numerical study, the time-dependent temperature distribution of the entire solid monolith structure and the two-dimensional laminar reactive flow fields in the single monolith channels are simulated. A multi-step heterogeneous reaction mechanism is used, and the surface coverage with adsorbed species is calculated as function of the position in the monolith. During light-off, complete oxidation of methane to water and carbon dioxide occurs initially. Then, synthesis gas selectivity slowly increases with rising temperature. © 2003 Elsevier Science Ltd. All rights reserved.

Keywords: Reaction Engineering; Multiphase reactions; Kinetics; Simulation; Partial oxidation; Synthesis gas

1. Introduction

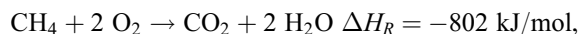
In the last few years, there is an increasingly strong interest in the catalytic partial oxidation of methane, the main component of natural gas (Hickman & Schmidt, 1993; Buyevskaya, Wolf, & Baerns, 1994; Heitnes, Lindeberg, Rokstad, & Holmen, 1995; Mallens, Hoebink, & Marin, 1997; Deutschmann & Schmidt, 1998; Bodke, Bharadwaj, & Schmidt, 1998; Vesper & Frauhammer, 2000). This interest is motivated by a strong demand for compact and low-capital-cost reactors for the conversion of natural gas to liquids and the production of hydrogen. Even though, a large variety of methods have been studied to find an efficient route for the direct conversion of methane to higher hydrocarbons (Belgued, Amariglio, Pareja, Ameriglio, & Saint-Just, 1992; Choudhary, Rajput, & Rane, 1992; Baerns, 1993; Wolf, Deutschmann, Behrendt, & Warnatz, 1999; Li, Borry, & Iglesia, 2001), no process has been discovered yet that has the potential to substitute the formation of synthesis gas, that is a mixture of hydrogen and carbon monoxide,

as a first step on the way from methane to higher hydrocarbons. Thus, multi-step methane conversion via synthesis gas is still the route of choice. The production of synthesis gas, or shorter syngas, accounts for $\sim 60\%$ of the costs of the whole conversion process. Presently, the most important industrial route to syngas is steam reforming of methane. This process is carried out in large-sized reactors with high energy demand.

Catalytic partial oxidation (CPO) of methane over noble metals, in particular rhodium, offers a promising alternative. This slightly exothermic reaction is globally written as



Since oxygen is available the highly exothermic complete oxidation of methane,



competes with the syngas production route. There is a still ongoing discussion whether syngas is formed via the direct route or via steam reforming after complete oxidation of methane. In a recent study, we supported a combination of both pathways (Deutschmann, Schwiedernoch, Maier, & Chatterjee, 2001a). The H_2 to CO ratio of ~ 2 in the product gas of the partial oxidation route is very favorable for subsequent methanol production or the Fischer–Tropsch process

* Corresponding author. Tel.: +49-6221-54-8886;
fax: +49-6221-54-8884.

E-mail address: deutschmann@iwr.uni-heidelberg.de
(O. Deutschmann).

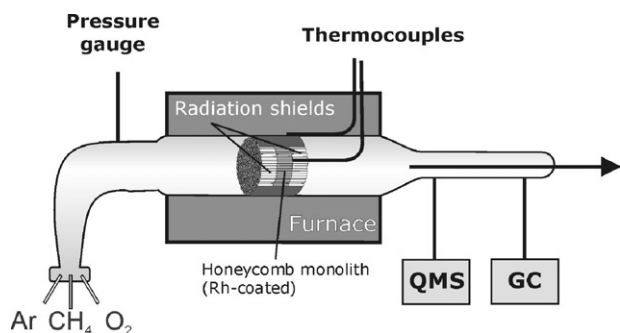


Fig. 1. Schematic of the experimental setup.

for synthetic liquid fuels. The provision of hydrogen for fuel cells, in particular in their application for the propulsion of future vehicles, presents a further driving force for a better and very compact syngas production technology. Syngas may also be added to the conventional vehicles' internal combustion engine during the start-up period in order to decrease pollutant emissions at a time when the catalytic converter does not work yet due to its initially low temperature. In those techniques, the understanding of the reactor behavior at transient conditions is often crucial for the overall performance, scale-up, reactor safety, and process optimization. Therefore, a strong interest exists in the application of reliable models and computational tools for the numerical simulation of the transient behavior of catalytic monoliths.

In this paper, we study the light-off of CPO of methane on rhodium/alumina at short contact times and atmospheric pressure. In the experiment, exit gas-phase temperature and species concentrations are monitored by thermocouples and mass spectroscopy, respectively. In the numerical study, a new approach is presented that permits the two- and three-dimensional simulation of the temperature distribution of the entire monolith coupled with two-dimensional laminar reactive flow field simulations of a representative number of single monolith channels. The latter predicts the gaseous velocity, species concentrations, temperature profiles, and surface coverage with adsorbed species based on a multi-step heterogeneous reaction mechanism.

2. Experiment

The light-off of the partial oxidation of methane in a rhodium coated monolith was investigated. The experiments were carried out in a flow reactor as schematically depicted in Fig. 1. The reactor consists of a 25 cm long quartz tube with a span diameter of 10 mm. An alumina honeycomb monolith is placed inside, composed of 24 channels with 0.43 mm² triangular cross-section, 5 mm in length.

The monolith is coated with rhodium. The Rh impregnation was achieved by saturating the monolith with an acidic

aqueous solution of Rh₂(SO₄)₃ · 4 H₂O followed by 24 h drying at 400 K, reduction in H₂ at 775 K, and finally calcination in air at 775 K for 18 h. This preparation procedure led to Rh loadings of about 3%-wt. Energy dispersive X-ray spectroscopy (EDX) measurements showed that no chlorine or sulfur compounds were left on the catalyst surface after impregnation.

Unloaded monoliths are placed in front of and behind the catalyst to reduce radiation heat loss. A ceramic cloth wound around the catalyst, 1 mm thick, prevents gas bypass. The entire reactor can be operated temperature-controlled by a furnace. The gas temperature at the exit of the catalytic monolith is monitored using a nickel/chrome/silicon-nickel/silicon (type N) thermocouple placed inside a thin quartz sheath to prevent catalytic reactions. A second thermocouple was used to measure the temperature of the outer glass wall. A ceramic insulation placed around the quartz tube reduces the heat loss of the entire reactor.

The reactor was operated at atmospheric pressure. In 80% Ar dilution, CH₄ and O₂ with a molar ratio of 1.7 were fed at 300 K into the preheated (700 K) monolith with a constant flow rate of 1.7 standard liter per minute (slpm) resulting in a flow velocity of 1.0 m/s. This flow rate corresponds to a gas hourly space velocity (GHSV) of 1.96×10^6 and a residence time of approximately 20 ms. The product composition was determined by gas chromatography (GC) and quadrupole mass spectroscopy (QMS). The latter was applied for transient measurements such as the ignition experiment of this study. The furnace is used to ignite the reaction by heating up the monolith using a temperature ramp of 5 K per minute. As soon as light off occurs, the furnace was turned off.

3. Modeling

In the model (sketched in Fig. 2), the reactive flow field in the single catalytic channels are coupled with the temperature distribution of the entire reactor for the description of the transient behavior of the monolith. The single channels are modeled by the steady-state, two-dimensional boundary-layer equations with transport coefficients that depend on composition and temperature. Surface and gas phase reactions are modeled by elementary-step based reaction mechanisms using the tools for reaction kinetics of the DETCHEM computer package (Deutschmann et al., 2001b). Along the channel, a varying surface coverage of adsorbed species is taken into account at the catalytic wall.

If the reactants' residence time in the monolith is shorter than 100 ms, it can be assumed that the time scales of the reactive flow and the solid's thermal respond are decoupled. Thus, time variations in the local monolith temperature can be neglected when calculating the fluid flow through single channels at a given time. Therefore, a time-independent formulation is used to describe the gaseous flow, while a

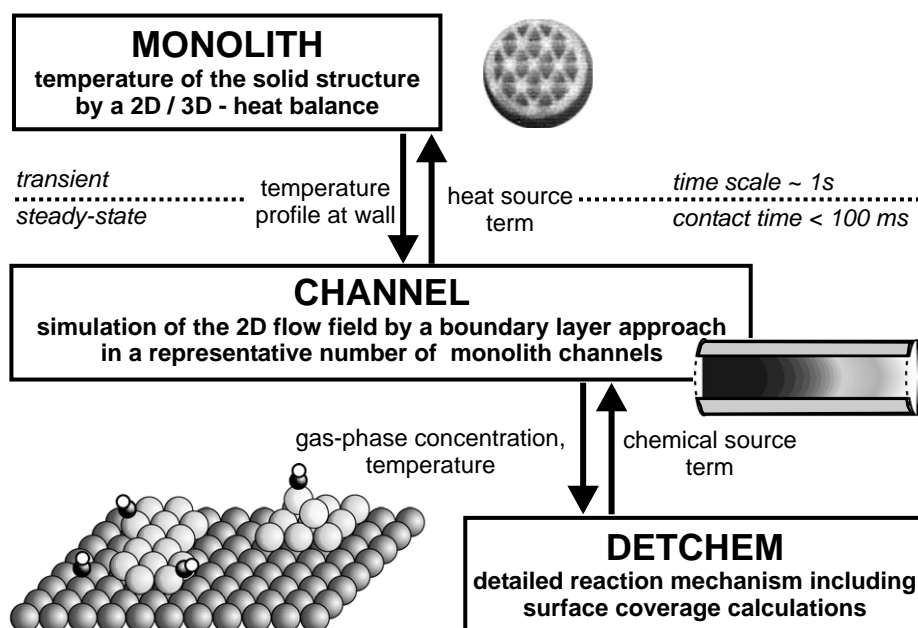


Fig. 2. Structure of the applied model.

transient heat conduction equation for the solid is solved (Jahn, Snita, Kubicek, & Marek, 1997). Hence, the numerical model for the simulation of the monolith consists of two linked modules, one for the simulation of the heat balance in the solid and one for the simulation of the flow field and chemistry in the single channels.

Despite the actual triangular shape of the monolith channels, a cylindrical channel model was applied. Given the inlet (velocity, temperature, species mass fractions) and boundary conditions (axial profile of the wall temperature), the two-dimensional flow field of the fluid can be calculated. However, the solution of the Navier–Stokes equations for the description of the laminar flow of chemically reacting flows is computationally expensive. Therefore, simpler models such as plug-flow or boundary-layer models are frequently used (Raja, Kee, Deutschmann, Warnatz, & Schmidt, 2000; Schlichting & Gersten, 1999). The boundary-layer approach is used in the DETCHEM^{CHANNEL} code (Deutschmann et al., 2001b; Tischer, Correa, & Deutschmann, 2001), which is applied in the present work.

In the boundary layer of a fluid near a surface, the convection is mainly directed parallel to the surface. The diffusive transport in the same direction diminishes in comparison with the one perpendicular to the surface. This effect becomes more significant as the axial gas velocity is increased, i.e. for higher Reynolds numbers as long as the flow is laminar. The results achieved by the boundary-layer model can be as accurate as the results from the full Navier–Stokes model at high but laminar flow rates (Raja et al., 2000). Mathematically, the character of the equations is simplified from elliptical to parabolic with a time-like coordinate along the channel axis. The set of equations in DETCHEM^{CHANNEL}

consists of conservation equations for:

total mass

$$\frac{\partial(r\rho u)}{\partial z} + \frac{\partial(r\rho v)}{\partial r} = 0, \quad (1)$$

mass of species i

$$\frac{\partial(r\rho u Y_i)}{\partial z} + \frac{\partial(r\rho v Y_i)}{\partial r} = -\frac{\partial}{\partial r}(r j_i) + r \dot{\omega}_i, \quad (2)$$

axial momentum

$$\frac{\partial(r\rho u u)}{\partial z} + \frac{\partial(r\rho v u)}{\partial r} = -r \frac{\partial p}{\partial z} + \frac{\partial}{\partial r} \left(\mu r \frac{\partial u}{\partial r} \right), \quad (3)$$

and enthalpy

$$\frac{\partial(r\rho u h)}{\partial z} + \frac{\partial(r\rho v h)}{\partial r} = r u \frac{\partial p}{\partial z} + \frac{\partial}{\partial r} \left(\lambda r \frac{\partial T}{\partial r} \right) - \frac{\partial}{\partial r} \left(\sum_i r j_i h_i \right). \quad (4)$$

The transport coefficients for radial diffusion (μ, λ) and the species diffusion fluxes j_i depend on temperature and species composition. Surface and gas-phase reaction source terms ($j_{i, \text{surf}}, \dot{\omega}_i$) are modeled by elementary-step based reaction mechanisms using the corresponding module of the DETCHEM program package (Deutschmann et al., 2001b; Tischer et al., 2001). The model of the catalytic reactions on the inner channel wall accounts for a varying surface coverage of adsorbed species along the channel, which is given by

$$\Theta_i = \frac{c_i \sigma_i}{\Gamma}, \quad (5)$$

Table 1

Material properties of the catalytic monolith and the insulation used in the model (Lide, 1994)

Physical properties	Alumina monolith	Insulation/quartz
Porosity	0.368	
Heat conduction λ_{rad} [W/(m K)]	20 ^a /12.6 ^b	1.36
Density ρ [kg/m ³]	3500 ^a /2214 ^b	2205
Heat capacity c_p [J/(kg K)]	850	730

^aFor compact material, porosity = 0.

^bIncluding porosity.

where Θ_i is the coverage with species i , c_i the concentration of species i on the surface, in, e.g., mol/m², σ_i the number of occupied adsorption sites by species i , and Γ the surface site density, i.e., the number of adsorption sites per catalytic surface area, given in, e.g., mol/m².

Catalytic reactions at the surface are taken into account in terms of a diffusive surface flux $j_{i,\text{surf}}$ in Eq. (2) at the boundary by

$$j_{i,\text{surf}} = F_{\text{cat}/\text{geo}} \cdot M_i \dot{s}_i. \quad (6)$$

Here, M_i is the molar mass of species i , $F_{\text{cat}/\text{geo}}$ is the ratio of catalytically active surface area to geometrical surface area of the channel. The reaction rate \dot{s}_i is then described by

$$\dot{s}_i = \sum_{k=1}^{K_s} \nu_{ik} k_{fk} \prod_{j=1}^{N_g+N_s} c_j^{\nu_{jk}}, \quad (7)$$

with K_s the number of heterogeneous reactions, N_g/N_s the number of gas-phase/surface species, ν the stoichiometric coefficients, and the rate coefficient

$$k_{fk} = A_k T^{\beta_k} \exp\left[\frac{-E_{ak}}{RT}\right] f_k(\Theta_1, \dots, \Theta_{N_s}), \quad (8)$$

including an additional coverage dependence in terms of

$$f_k(\Theta_1, \dots, \Theta_{N_s}) = \prod_{i=1}^{N_g} \Theta_i^{\mu_{ik}} \exp\left[\frac{\varepsilon_{ik} \Theta_i}{RT}\right]. \quad (9)$$

Given the inlet conditions, the boundary-layer equations are solved in a single sweep of integration along the axial direction by a method-of-lines procedure. The radial derivatives are discretized by a finite-volume method. The resulting differential-algebraic equation system is integrated using the semi-implicit extrapolation solver LIMEX (Deuffhardt, Hairer, & Zugk, 1987).

The thermal behavior of the monolithic structure is simulated by the computer code DETCHEM^{MONOLITH} (Deutschmann et al., 2001b; Tischer et al., 2001), which applies the model of a two-dimensional temperature equation:

$$\frac{\partial T}{\partial t} = \nabla^2 \left(\frac{\lambda T}{\rho c_p} \right) + \frac{q}{\rho c_p}. \quad (10)$$

The material properties (density ρ , heat capacity c_p and thermal conductivity λ) are functions of the material (monolith or insulation) as given in Table 1. Heat losses due

to conduction, convection, and thermal radiation at the exterior walls of the monolith can be included.

The monolith and the channel calculations are coupled by the heat source terms q in the temperature equation.

$$q = -\sigma \cdot 2\pi r \lambda \left. \frac{\partial T_{\text{gas}}}{\partial r} \right|_{\text{surf}}. \quad (11)$$

Therefore, each axial temperature profile is applied as a boundary condition for a channel calculation, which returns the heat flux from the gas phase into the monolith due to convection and chemical heat release. Since the channel calculation is the step consuming most time, only a representative number of channels is calculated explicitly. In the present simulation, five channels are used being at the radial position of 0, 1.5, 3, 4.5, 6 mm. The calculation is computationally parallelized and can be extended to a larger number of channels if needed.

For the spatial discretization of the transient temperature equation, a finite volume approach is used. Either the LIMEX (Deuffhardt et al., 1987) or LSODE (Hindmarsh, 1983) solver can be chosen for the integration of the resulting ordinary differential equation system. Based on these models, the computational tool predicts the transient, two-dimensional distributions of temperature and species concentrations.

A detailed surface reaction mechanism is applied to model the oxidation of methane on rhodium. Since this mechanism also takes intermediate steps and species into account, further global reactions such as steam or CO₂ reforming are automatically included. The detailed surface reaction mechanism is based on our former study on steady-state partial oxidation of methane on Rh (Deutschmann et al., 2001a). In the ignited steady-state, the total surface coverage is low. Therefore, the coverage dependence of the rate coefficients was neglected in the former study. However, before ignition the surface usually reveals a high coverage with adsorbed species. Therefore, in the present work, coverage dependent activation energies were chosen for the desorption of CO and oxygen, which is also supported by a recent SFG (sum-frequency generation) study at atmospheric pressure (Pery et al., 2002). The here applied heterogeneous reaction mechanism consists of 38 reactions among 6 gas phase species and 11 surface species and is given in Table 2.

The simulation also includes a detailed gas-phase reaction mechanism (Baulch et al., 1992). However, gas phase reactions are found to be not significant at the conditions chosen.

Based on these models, the recently developed computational tool DETCHEM^{MONOLITH} predicts the two/three-dimensional temperature distribution in the solid structure of the monolith and the two-dimensional gas-phase temperature, species concentrations, and velocity distributions in the single channels as function of time. Furthermore, time-varying inlet conditions (temperature, species concentrations, flow velocity) can be specified as long as the

Table 2
Surface reaction mechanism

			A/[cm,mol,s]	E _a /[kJ/mol]
1. Adsorption				
H ₂ + Rh(s) + Rh(s)	→ H(s)	+H(s)	1.000 · 10 ⁻⁰²	s.c. ^a
O ₂ + Rh(s) + Rh(s)	→ O(s)	+O(s)	1.000 · 10 ⁻⁰²	s.c. ^a
CH ₄ + Rh(s)	→ CH ₄ (s)		8.000 · 10 ⁻⁰³	s.c. ^a
H ₂ O + Rh(s)	→ H ₂ O(s)		1.000 · 10 ⁻⁰¹	s.c. ^a
CO ₂ + Rh(s)	→ CO ₂ (s)		1.000 · 10 ⁻⁰⁵	s.c. ^a
CO + Rh(s)	→ CO(s)		5.000 · 10 ⁻⁰¹	s.c. ^a
2. Desorption				
H(s) + H(s)	→ Rh(s)	+Rh(s) + H ₂	3.000 · 10 ⁺²¹	77.8
O(s) + O(s)	→ Rh(s)	+Rh(s) + O ₂	1.300 · 10 ⁺²²	355.2-280θ _{O(s)}
H ₂ O(s)	→ H ₂ O	+Rh(s)	3.000 · 10 ⁺¹³	45.0
CO(s)	→ CO	+Rh(s)	3.500 · 10 ⁺¹³	133.4-15θ _{CO(s)}
CO ₂ (s)	→ CO ₂	+Rh(s)	1.000 · 10 ⁺¹³	21.7
CH ₄ (s)	→ CH ₄	+Rh(s)	1.000 · 10 ⁺¹³	25.1
3. Surface reactions				
H(s) + O(s)	→ OH(s)	+Rh(s)	5.000 · 10 ⁺²²	83.7
OH(s) + Rh(s)	→ H(s)	+O(s)	3.000 · 10 ⁺²⁰	37.7
H(s) + OH(s)	→ H ₂ O(s)	+Rh(s)	3.000 · 10 ⁺²⁰	33.5
H ₂ O(s) + Rh(s)	→ H(s)	+OH(s)	5.000 · 10 ⁺²²	104.7
OH(s) + OH(s)	→ H ₂ O(s)	+O(s)	3.000 · 10 ⁺²¹	100.8
H ₂ O(s) + O(s)	→ OH(s)	+OH(s)	3.000 · 10 ⁺²¹	171.8
C(s) + O(s)	→ CO(s)	+Rh(s)	3.000 · 10 ⁺²²	97.9
CO(s) + Rh(s)	→ C(s)	+O(s)	2.500 · 10 ⁺²¹	169.0
CO(s) + O(s)	→ CO ₂ (s)	+Rh(s)	1.400 · 10 ⁺²⁰	121.6
CO ₂ (s) + Rh(s)	→ CO(s)	+O(s)	3.000 · 10 ⁺²¹	115.3
CH ₄ (s) + Rh(s)	→ CH ₃ (s)	+H(s)	3.700 · 10 ⁺²¹	61.0
CH ₃ (s) + H(s)	→ CH ₄ (s)	+Rh(s)	3.700 · 10 ⁺²¹	51.0
CH ₃ (s) + Rh(s)	→ CH ₂ (s)	+H(s)	3.700 · 10 ⁺²⁴	103.0
CH ₂ (s) + H(s)	→ CH ₃ (s)	+Rh(s)	3.700 · 10 ⁺²¹	44.0
CH ₂ (s) + Rh(s)	→ CH(s)	+H(s)	3.700 · 10 ⁺²⁴	100.0
CH(s) + H(s)	→ CH ₂ (s)	+Rh(s)	3.700 · 10 ⁺²¹	68.0
CH(s) + Rh(s)	→ C(s)	+H(s)	3.700 · 10 ⁺²¹	21.0
C(s) + H(s)	→ CH(s)	+Rh(s)	3.700 · 10 ⁺²¹	172.8
CH ₄ (s) + O(s)	→ CH ₃ (s)	+OH(s)	1.700 · 10 ⁺²⁴	80.3
CH ₃ (s) + OH(s)	→ CH ₄ (s)	+O(s)	3.700 · 10 ⁺²¹	24.3
CH ₃ (s) + O(s)	→ CH ₂ (s)	+OH(s)	3.700 · 10 ⁺²⁴	120.3
CH ₂ (s) + OH(s)	→ CH ₃ (s)	+O(s)	3.700 · 10 ⁺²¹	15.1
CH ₂ (s) + O(s)	→ CH(s)	+OH(s)	3.700 · 10 ⁺²⁴	158.4
CH(s) + OH(s)	→ CH ₂ (s)	+O(s)	3.700 · 10 ⁺²¹	36.8
CH(s) + O(s)	→ C(s)	+OH(s)	3.700 · 10 ⁺²¹	30.1
C(s) + OH(s)	→ CH(s)	+O(s)	3.700 · 10 ⁺²¹	145.5

^aValue sticking coefficient. $\Gamma = 2.72 \times 10^{-9}$ mol/cm² Eq. (5). Nomenclature given in (Deuschmann et al., 2001b). This mechanism can also be downloaded from: <http://reaflow.iwr.uni-heidelberg.de/~dmann>.

conditions vary at a time scale that is larger than the residence time.

4. Results and discussion

4.1. Temperature and reaction kinetics in the catalytic monolith during light-off

The CH₄/O₂/Ar mixture, initially at room temperature and atmospheric pressure, was continuously fed into the reactor. The volumetric CH₄/O₂-ratio was 1.7 with 80% Ar dilution. The initially cold monolith was slowly heated up by increasing the temperature of the surrounding

furnace. A temperature ramp of 5 K per minute was applied. While no conversion occurred at low temperature, an increasing but small amount of methane and oxygen was consumed above 600 K leading to some water and carbon dioxide formation, no syngas is formed. Ignition was then experimentally determined by the suddenly rapid increase in methane and oxygen conversion, and temperature. This process was combined with the onset of syngas formation. At the ignition point, the furnace was switched off. The precise evaluation of the heat transport between reactor and furnace surely is a challenge in the current experimental configuration.

Fig. 3 reveals the numerically predicted temperature distribution in the solid monolithic structure as function of time

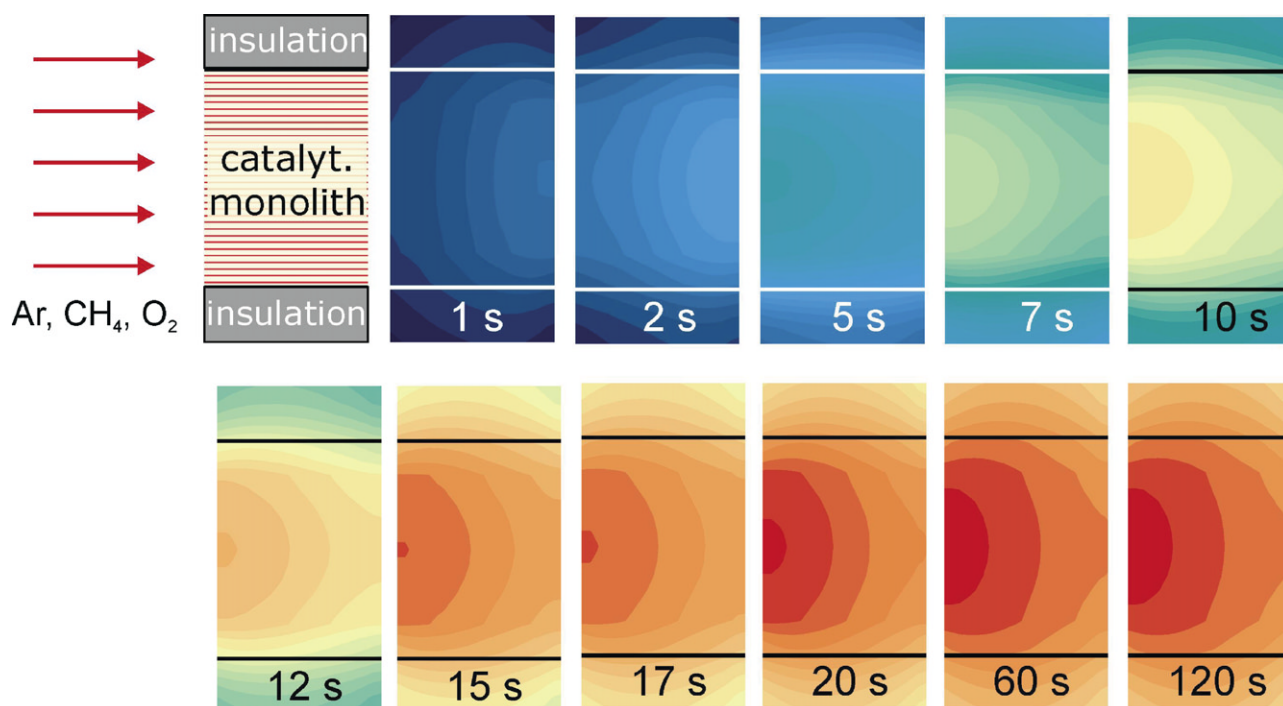


Fig. 3. (a) Numerically predicted temperature distribution in the solid structure of the catalytic monolith and the thermal insulation during light-off. The maximum (red) and minimum (blue) temperatures are 675 and 925 K, respectively. Ignition starts at time 0 s, see Fig. 6.

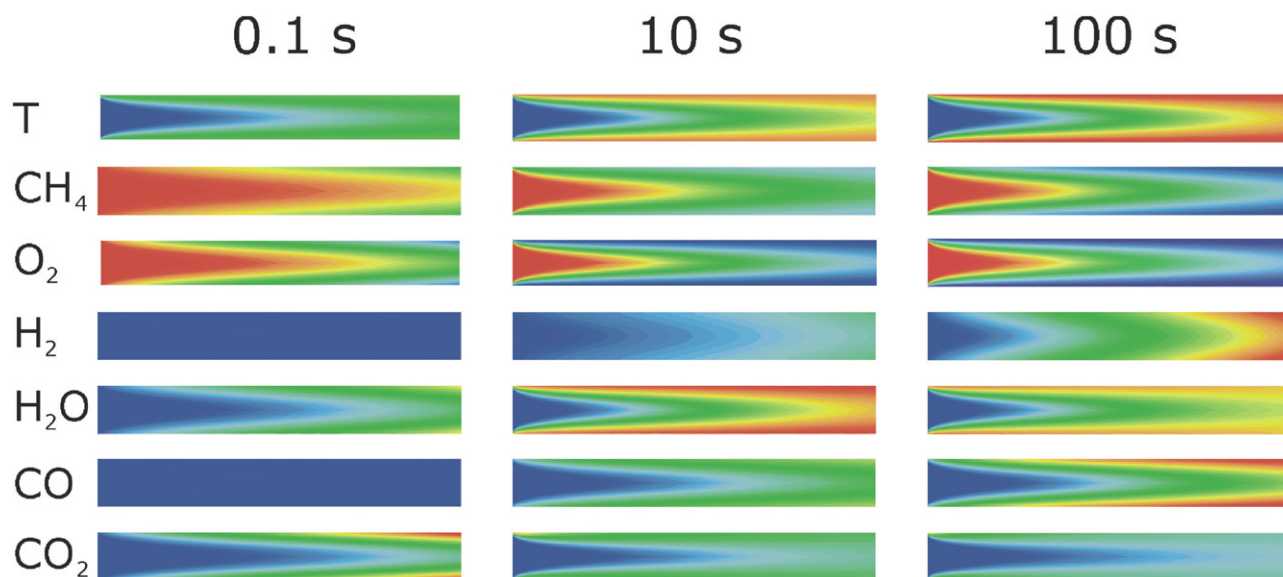


Fig. 4. Gas-phase temperature and species mole fractions in a single channel in the monolith's centerline 0.01, 10, and 100 s after ignition. The temperature range is 385–900 K, the ranges of the mole fractions are CH_4 : 0.043–0.094, O_2 : 0–0.055, H_2 : 0–0.0412, H_2O : 0–0.058, CO : 0–0.042, CO_2 : 0–0.056.

during light-off. The temperature ranges from 675 K (blue) to 925 K (red). At ignition, the front face of the preheated monolith (furnace temperature is 700 K) is cooled down by the incoming gas (368 K). At the monolith exit, the temperature remains high enough (700 K) to lead to light-off. Here, at first total oxidation of CH_4 to CO_2 and H_2O occurs as revealed by Fig. 4 showing the gas-phase temperature

and species concentration profiles at 0.1, 10, and 100 s after ignition. The highly exothermic reaction produces heat, which leads to an increase of the temperature further upstream. There is no H_2 and CO produced at this moment.

The main reaction zone moves towards the monolith entrance in the first few seconds after ignition (Fig. 3). After ten seconds, the maximum of CO_2 production already

occurs at the channel entrance (Fig. 4). Since the temperature rises and oxygen is rapidly consumed, some CO is formed at the channel exit. The hottest part of the reactor is now at the front face, where the highly exothermic total oxidation occurs, also causing a downstream heat transfer. The only slightly exothermic direct partial oxidation occurs at the catalyst exit. At 10 s the temperature is high enough for hydrogen formation, again beginning at the exit of the channel.

Later, with higher temperatures, hydrogen and CO formation increases while CO₂ and H₂O formation decreases. After approximately 60 seconds, conversion and selectivity reach steady state. While the maximum of the solid temperature still is at the catalyst entrance, the gas-phase reaches its maximum temperature, averaged over the radial coordinate, at the monolith exit. While most of the oxygen is consumed in the first part of the reactor leading to total oxidation of methane, most of the syngas, in particular, hydrogen, is formed further downstream. CO formation starts before hydrogen formation. Hydrogen is formed via direct partial oxidation and via steam reforming. CO is formed via direct partial oxidation and steam reforming as well but apparently not via CO₂ reforming. The endothermic steam reforming adds to the temperature decrease along the catalytic monolith, which is also caused by radial heat loss via the insulation.

The model includes the calculation of the surface coverage with adsorbed species along the catalytic channels as function of time. Fig. 5 reveals the computed surface coverages 0.1 and 10 s after ignition. Before ignition, the surface is mainly covered by oxygen blocking a high reaction rate, the system is controlled by surface reaction kinetics, in particular by the availability of adsorption sites for methane. The high oxygen sticking leads to rhodium oxides increasing the total amount of oxygen available for later reaction on the catalyst. The adsorption–desorption equilibrium for oxygen slowly shifts towards desorption with increasing temperature leading to more and more vacancies on the surface. These vacancies can be occupied by methane that decomposes during adsorption. The large number of reactive oxygen available (chemisorbed and in rhodium oxide) then leads to fast carbon monoxide formation and finally total oxidation. The temperature increase caused by the total oxidation reaction leads to a further shift of the adsorption–desorption equilibrium for oxygen towards desorption, and hence, to more available adsorption sites, self-accelerating the reaction, leading to ignition. Furthermore, the rhodium oxide is reduced during light-off. After ignition, the overall reaction is controlled by radial heat and mass transport as can be clearly seen by the steep radial gradients in the gas-phase profiles of Fig. 4. The total surface coverage is lower and significant oxygen coverage can only be seen at the catalyst entrance where complete oxidation occurs. Further downstream, the oxygen coverage decreases rapidly, all adsorbed oxygen here comes from re-adsorbed water. Oxygen on the catalyst is only sufficient for CO formation.

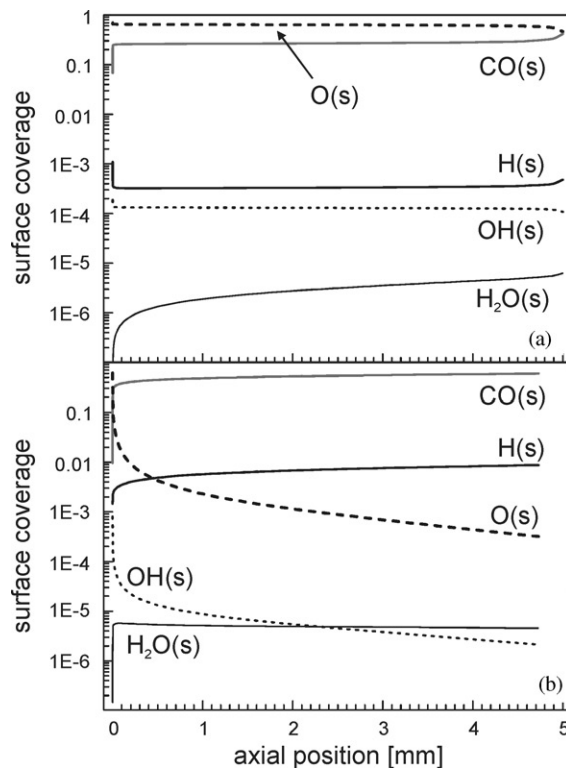


Fig. 5. Surface coverage of CO, O, H, OH, H₂O on rhodium 0.1 s (a) and 10 s (b) after ignition.

Carbon monoxide and hydrogen are desorbed before they are oxidized completely.

Since the simulation computes the processes in the single channels at various radial positions, here five, the impact of radial temperature gradients over the entire monolith on the conversion and selectivity in the single channels can be elucidated. According to the temperature profiles as shown in Fig. 3 the conversion and syngas selectivity are lower in the outer regions where the temperature is lower (not shown).

4.2. Experiments versus simulation

In Fig. 6, the numerically predicted gas-phase temperature, CH₄ and O₂ conversion and syngas selectivity at the catalyst exit are compared with the experimentally derived data. The simulation of the exit gas-phase temperature is in good agreement with the experimental results. The simulated surface temperature at the catalyst exit is slightly higher than the gas-phase temperature. The predicted ignition gas-phase temperature at the catalyst exit was slightly lower than the experimentally determined temperature, which is still in the error bar of the measurement. The slower temperature rise in the experiment is probably due to the heat capacity of the thin quartz tube, in which the thermocouple was placed. The predicted temperature rather increases like the adiabatic reactor temperature, which is derived from the experimentally

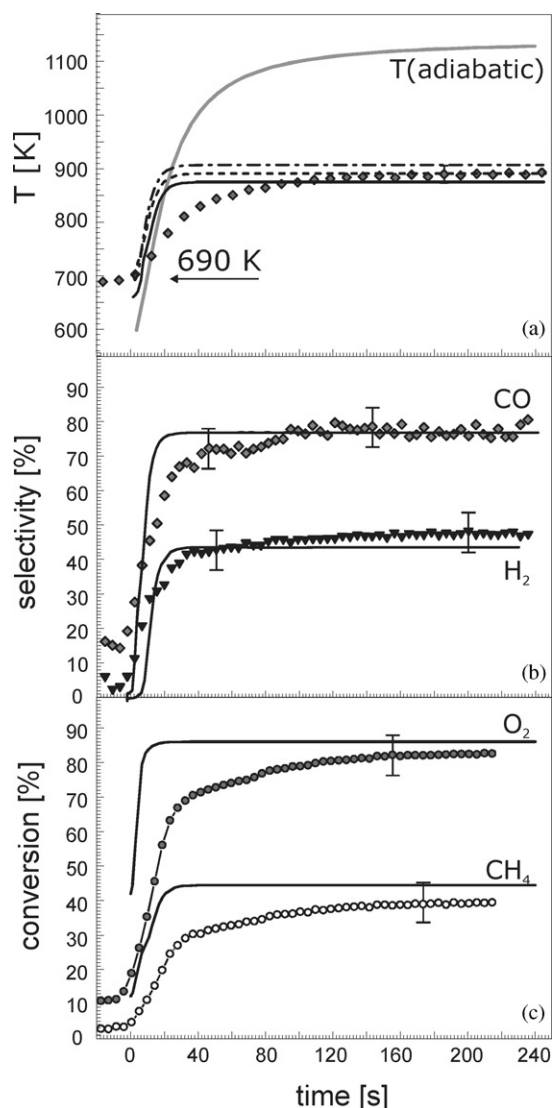


Fig. 6. (a) Temperature profile during light-off. Diamonds represent the measured gas-phase temperature at the exit of the catalytic monolith. The numerically predicted gas-phase temperature is depicted by a solid black line, the temperature of the catalytic surface at the entrance by a dashed-dotted line and at the exit by a dashed line. (b) H₂ and CO selectivity and (c) O₂ and CH₄ conversion as function of time; symbols/lines represent the experimental/numerical data, respectively.

exit product composition assuming overall adiabatic reactor conditions. As mentioned above, the specification of the accurate heat source/loss term at the outer wall of the reactor's tube is a weak point in the simulation and needs further consideration.

Numerically predicted H₂ and CO selectivity (Fig. 6b) and the O₂ and CH₄ conversion (Fig. 6c) agree well with the experimentally derived data. Only little CO and no H₂ is produced at the ignition point. Then, syngas selectivity increases rapidly. However, the simulation reaches steady state faster than the experimentally determined data. The temporal resolution of the used quadrupole mass spectrometer is several seconds explaining the deviations.

A comparison of the present numerical simulation of the single channel using the (parabolic) boundary layer model with a simulation applying a fully elliptic code (Fluent plus DETCHEM, Deutschmann et al., 2001b), which accounts for axial diffusion, lead to the same results. Therefore, the deviations between experiment and simulation are not caused by the simplifications of the boundary layer approach.

Since the channels of the monolith have the relatively large diameter of 0.74 mm and the monolith is only 5 mm in length, we see oxygen breakthrough in the experiment and simulation. The reaction is not completed yet, which explains the low syngas selectivity in comparison to many other studies. The objective of this study was rather gaining a better understanding of the reactor than optimizing the syngas yield. It is even better to have lower conversion, in particular oxygen breakthrough, for model validation.

5. Conclusions

The light-off of catalytic partial oxidation of methane on a rhodium coated alumina monolith was experimentally studied in a flow reactor at short contact times using mass spectroscopy and thermocouples. At ignition, only total oxidation of methane to carbon dioxide and water occurs. Then, the hydrogen and carbon monoxide selectivity increases with rising temperature.

A recently developed computer code, DETCHEM^{MONOLITH}, was applied to study the transient behavior of the monolith during light-off numerically. The detailed simulation was based on the solution of the two-dimensional heat balance of the solid monolith structure coupled with two-dimensional flow field simulations of five representative monolith channels. The model includes elementary-step based reaction mechanisms for the heterogeneous and potential homogeneous reactions.

The simulation revealed the movement of the reaction zone from the rear face to the front face of the monolith during ignition. A strong competition between direct partial oxidation, total oxidation, and steam reforming occurs in the reactor. The surface is covered by oxygen before ignition. At steady state, oxygen is the primary adsorbed species in the catalyst entrance region, where total oxidation occurs. Further downstream, the oxygen coverage decreases rapidly, and steam reforming leads to an increase in syngas selectivity.

The numerically predicted temperatures, conversion, and selectivity agree well with the experimentally determined data. The developed computer code was shown to be able to describe the transient behavior of the catalytic monolith in detail and led to a better understanding of the intrinsic chemical reactions and their interaction with mass and heat transport in the catalytic reactor. The computer code is currently applied to study a variety of further catalytic monoliths such as automotive catalytic converters and catalytic combustion stages.

Notation

c_i	concentration
c_p	specific heat
f_k	coverage dependency function
h_i	enthalpy of species i
h	enthalpy of the mixture
p	pressure
q	heat source term
j_i	diffusive flux including surface flux
k_{fk}	reaction rate
r	radial spatial coordinate
\dot{s}_i	reaction rate
t	time
u	axial velocity
v	radial velocity
z	axial spatial coordinate
A_k	pre-exponential factor
E_{ak}	activation energy
$F_{cat/geo}$	surface scaling factor (catalytic/geometric)
K_s	number of surface reactions
M_i	molar Mass
N_g	number of gas-phase species
N_s	number of surface species
R	gas constant
T	temperature
Y_i	mass fraction of species i

Greek letters

β_k	temperature exponent
ε_i	coverage dependent activation energy
λ	thermal conductivity
μ	viscosity
ν_{ik}	stoichiometric coefficients
ρ	density
σ	channel density
σ_i	number of occupied adsorption sites
$\dot{\omega}_i$	gas phase reaction source term
Γ	surface site density
Θ_i	surface coverage

Acknowledgements

We would like to thank Jürgen Warnatz (Heidelberg University) for his continuous support of our work on heterogeneous catalysis. Jürgen Wolfrum's and Hans-Robert Volpp's (Heidelberg University) help in setting up the experiment is very appreciated. This work was financially supported by the Deutsche Forschungsgemeinschaft (DFG), J. Eberspächer GmbH & Co, Esslingen, Germany, and Conoco Inc. Ponca City, OK, USA.

References

- Baerns, M. (1993). Oxidative coupling of methane for utilization of natural gas. In H.I. de Lesa et al. (Eds.), *Chemical reactor technology for environmental safe reactors and products* (pp. 283–316). Dordrecht: Kluwer Academic Publishers.
- Baulch, D. L., Cobos, C. J., Cox, R. A., Esser, C., Frank, P., Just, T., Kerr, J. A., Pilling, M. P., Troe, J., Walker, R. W., & Warnatz, J. (1992). *Journal of Physical Chemical Reference Data*, 21, 441.
- Belgued, M., Amariglio, H., Pareja, P., Ameriglio, A., & Saint-Just, J. (1992). Low temperature catalytic homologation of methane on platinum, ruthenium and cobalt. *Catalysis Today*, 13, 337–445.
- Bodke, A. S., Bharadwaj, S. S., & Schmidt, L. D. (1998). The effect of ceramic supports on partial oxidation of hydrocarbons over noble metal coated monoliths. *Journal of Catalysis*, 179, 138–149.
- Buyevskaya, O. V., Wolf, D., & Baerns, M. (1994). Rhodium—catalyzed partial oxidation of methane to CO and H₂. Transient studies on its mechanism. *Catalysis Letters*, 29, 249–260.
- Choudhary, V. R., Rajput, A. M., & Rane, V. H. (1992). Low-temperature catalytic selective partial oxidation of methane to CO and H₂ over Ni/Yb₂O₃. *Journal of Physical Chemistry*, 96, 8686–8688.
- Deuflhard, P., Hairer, E., & Zguck, J. (1987). One-step and extrapolation methods for differential-algebraic systems. *Numerische Mathematik*, 51, 501–516.
- Deutschmann, O., Correa, C., Tischer, S., Chatterjee, D., Kleditzsch, S. & Warnatz, J. (2001b). DETCHEM Version 1.4.2. <http://reaflow.iwr.uni-heidelberg.de/~dmann/DETCHEM.html>.
- Deutschmann, O., & Schmidt, L. D. (1998). Modeling the partial oxidation of methane in a short contact time reactor. *A.I.Ch.E. Journal*, 44, 2465–2476.
- Deutschmann, O., Schwiedernoch, R., Maier, L., & Chatterjee, D. (2001a). Natural gas conversion in monolithic catalysts: Interaction of chemical reactions and transport phenomena. Studies in surface science and catalysis. In E. Iglesia., J. J. Spivey, T. H. Fleisch (Eds.), *Natural gas conversion VI*, vol. 136 (p. 215). Amsterdam: Elsevier.
- Heitnes, K., Lindeberg, S., Rokstad, O. A., & Holmen, A. (1995). Catalytic partial oxidation of methane to synthesis gas. *Catalysis Today*, 24, 211–216.
- Hickman, D. A., & Schmidt, L. D. (1993). Steps in CH₄ Oxidation on Pt and Rh surfaces: High temperature reactor simulation. *A.I.Ch.E. Journal*, 39(7), 1164–1177.
- Hindmarsh, A. C. (1983). Scientific computing (pp. 55–64) Amsterdam.
- Jahn, R., Snita, D., Kubicek, M., & Marek, M. (1997). 3D-modeling of monolith reactors. *Catalysis Today*, 38, 39–46.
- Li, L., Borry, R., & Iglesia, E. (2001). Reaction-transport simulations of non oxidative methane conversion with continuous hydrogen removal—homogeneous-heterogeneous reaction pathways. *Chemical Engineering Science*, 56, 1869–1881.
- Lide, D. R. (Ed.) (1994). *CRC handbook of chemistry and physics* (75th ed.). Boca Raton: CRC Press.
- Mallens, E. P. J., Hoebink, J. H. B., & Marin, G. B. (1997). The reaction mechanism of the partial oxidation of methane to synthesis gas: A transient kinetic study over rhodium and a comparison with platinum. *Journal of Catalysis*, 167, 43–46.
- Pery, T., Schweitzer, M. G., Volpp, H.-R., Wolfrum, J., Ciossu, L., Deutschmann, O., & Warnatz, J. (2002). Sum-frequency generation in situ study of CO adsorption and catalytic CO oxidation on rhodium at elevated pressures. *Proceedings of Combustion Institute*, 29, in press.
- Raja, L. L., Kee, R. J., Deutschmann, O., Warnatz, J., & Schmidt, L. D. (2000). A critical evaluation of Navier–Stokes, boundary-layer, and plug-flow models for the simulation of flow and chemistry in a catalytic combustion honeycomb channel. *Catalysis Today*, 59, 47–60.

- Schlichting, H., & Gersten, K. (1999). In *Boundary-Layer Theory* (8th ed.). Heidelberg: Springer.
- Tischer, S., Correa, C., & Deutschmann, O. (2001). Transient three-dimensional simulation of a catalytic combustion monolith using detailed models for heterogeneous and homogeneous reactions and transport phenomena. *Catalysis Today*, 69, 57–62.
- Veser, G., & Frauhammer, J. (2000). Modelling steady state and ignition during catalytic methane oxidation in a monolith reactor. *Chemical Engineering Science*, 55, 2271–2286.
- Wolf, M., Deutschmann, O., Behrendt, F., & Warnatz, J. (1999). Kinetic model of an oxygen-free methane conversion on a platinum catalyst. *Catalysis Letters*, 61, 15–25.